Molecular Organization and Dynamic Behaviour of Arene Cluster Complexes in the Solid State. Crystal Structures of $[Os_4H_2(CO)_{10}(\eta^6\text{-}C_6H_5Me)]$, $[Os_4H_2(CO)_{10}(\eta^6\text{-}C_6H_4Me_2)]$ and $[Ru_6C(CO)_{14}(\eta^6\text{-}C_6H_3Me_3\text{-}1,3,5)]$†

Dario Braga,*[a] Fabrizia Grepioni,[a] Brian F. G. Johnson,[b] Hong Chen[c] and Jack Lewis*[c]

[a] *Dipartimento di Chimica 'G. Ciamician', Università di Bologna, Via Selmi 2, 40126 Bologna, Italy*

[b] *Department of Chemistry, University of Edinburgh, West Mains Road, Edinburgh EH9 3JJ, UK*

[c] *University Chemical Laboratory, Lensfield Road, Cambridge CB2 1EW, UK*

The molecular organization in crystals of the tetranuclear arene clusters $[Os_4H_2(CO)_{10}(\eta^6\text{-arene})]$ (arene = C_6H_6, C_6H_5Me, $C_6H_4Me_2$-*o* or -*m*) and of the hexanuclear species $[Ru_6C(CO)_{14}(\eta^6\text{-}C_6H_5Me)]$, $[Ru_6C(CO)_{14}(\eta^6\text{-}C_6H_3Me_3\text{-}1,3,5)]$ and $[Ru_6C(CO)_{11}(\mu_3\text{-}\eta^2\text{:}\eta^2\text{:}\eta^2\text{-}C_6H_6)(\eta^6\text{-}C_6H_6)]$ has been investigated by means of packing potential-energy calculations and computer graphics analysis. Attention is focused on the relationship between the shape, size and geometry of these molecules and the ease of reorientational motion of the arene fragments in the solid state. The crystal structures of $[Os_4H_2(CO)_{10}(\eta^6\text{-}C_6H_5Me)]$ and $[Os_4H_2(CO)_{10}(\eta^6\text{-}C_6H_4Me_2)]$ have been determined by X-ray diffraction and that of $[Ru_6C(CO)_{14}(\eta^6\text{-}C_6H_3Me_3\text{-}1,3,5)]$ redetermined.

In previous papers we have shown that much can be learned of the solid-state properties of organometallic compounds by studying the packing modes that the molecules adopt and also about the relationship between the molecular organization in the lattice and the occurrence of dynamic phenomena in the solid state.[1,2] It is well understood that unsaturated organic fragments co-ordinated to metal centres are able to undergo rotational motion in the solid state. It has been demonstrated that the ease with which reorientation may occur is essentially a function of the shape of the fragment, *e.g.* the more regular the shape (say disk-like benzene, cyclopentadienyl, hexamethylbenzene ligands) the easier is the reorientational phenomenon. On the contrary, when the fragments are less regular and present 'bumps' or cavities [toluene, mesitylene, 1,2,4,5-tetramethylbenzene (durene), *etc.*] the intermolecular assembly is usually able to lock in the fragment and thereby prevent full rotational freedom.

Activation energies and/or potential-energy barriers to reorientation have been estimated for families of mononuclear complexes such as metallocenes, $M(CO)_3$(arene) species, bis-(arene) compounds, *etc.*[3,4]

More recently clear-cut evidence that arene reorientation may occur also in the polynuclear species $[Ru_3(CO)_9(\mu_3\text{-}\eta^2\text{:}\eta^2\text{:}\eta^2\text{-}C_6H_6)]$, $[Os_3(CO)_7(\mu_3\text{-}\eta^2\text{-}C_2Me_2)(\eta^6\text{-}C_6H_6)]$, and $[Os_3(CO)_8(\eta^2\text{-}C_2H_4)(\mu_3\text{-}\eta^2\text{:}\eta^2\text{:}\eta^2\text{-}C_6H_6)]$ has been provided by potential-energy barrier calculations within the atom–atom pairwise potential-energy approach.[5] In the case of $[Os_3(CO)_8(\eta^2\text{-}C_2H_4)(\mu_3\text{-}\eta^2\text{:}\eta^2\text{:}\eta^2\text{-}C_6H_6)]$ good agreement was found with the results of ^{13}C cross polarization magic angle spinning (CP MAS) NMR experiments.[6]

In this paper the possibility of reorientational motion in crystals of the arene clusters $[Os_4H_2(CO)_{10}(\eta^6\text{-}C_6H_6)]$ **1**, $[Os_4H_2(CO)_{10}(\eta^6\text{-}C_6H_5Me)]$ **2**, $[Os_4H_2(CO)_{10}(\eta^6\text{-}C_6H_4Me_2)]$ **3**,‡ $[Ru_6C(CO)_{14}(\eta^6\text{-}C_6H_5Me)]$ **4**, $[Ru_6C(CO)_{14}(\eta^6\text{-}C_6H_3Me_3\text{-}1,3,5)]$ **5** and $[Ru_6C(CO)_{11}(\mu_3\text{-}\eta^2\text{:}\eta^2\text{:}\eta^2\text{-}C_6H_6)(\eta^6\text{-}C_6H_6)]$ **6** has been explored. We have found that the relationship between the shape of the arene fragment and ease of reorientation of the type discussed above for crystalline mononuclear complexes can be transferred to polymetallic systems. Differences in the dynamic behaviour of mono- and poly-nuclear complexes would appear to arise mainly at the *intramolecular* level. The crystal packing of these molecular species has also been analysed by means of approximate potential-energy calculations and computer graphics.

For the purposes of this study the crystal structures of the novel species **2** and **3** have been determined, and that of **5** redetermined, by single-crystal X-ray diffraction studies. The main structural features of these species are discussed. In the cases of **1**, **4** and **6**, data available in the literature have been used.

Methodology

Our approach to crystal packing has its roots in the atom–atom pairwise potential-energy method[8] developed and still widely used in the field of organic solid-state chemistry.[9] The method is well documented and will therefore not be described here in great detail.

Use is made of the expression p.p.e. $= \Sigma_i\Sigma_j[A\exp(-Br_{ij}) - Cr_{ij}^{-6}]$, where p.p.e. represents a sort of packing potential energy (but see below) and r_{ij} the non-bonded atom–atom intermolecular distance. Index i in the summation runs over all atoms of one molecule (chosen as reference molecule) and j over the atoms of the surrounding molecules distributed according to crystal symmetry. A cut-off of 15 Å has been adopted in our calculations. The values of the coefficients A, B and C used have been taken from the literature[10] and discussed in previous papers.[1,2] The results of p.p.e. calculations are used to select the first-neighbouring molecules (hereafter named FNM) among the molecules surrounding the one chosen as reference (hereafter named RM) on the basis of the contribution to the

† *Supplementary data available:* see Instructions for Authors, *J. Chem. Soc., Dalton Trans.*, 1991, Issue 1, pp. xviii–xxii.

Non-SI unit employed: cal = 4.184 J.

‡ *Compounds* **2** and **3** were prepared by the same method as that described[7] for **1**.

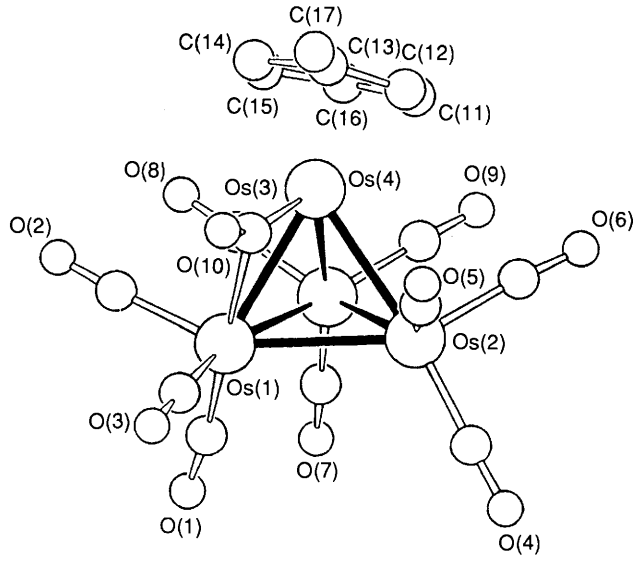

Fig. 1 The molecular structure of compound **2**, showing the atomic labelling scheme; H atoms are omitted for clarity, and the C atoms of the CO groups bear the same numbering as that of the corresponding O atoms

Table 1 Relevant bond distances (Å) and angles (°) for compound **2**

Os(1)–Os(2)	2.963(1)	C(11)–C(12)	1.42(3)
Os(1)–Os(3)	2.763(1)	C(12)–C(13)	1.37(3)
Os(1)–Os(4)	2.811(1)	C(13)–C(14)	1.44(3)
Os(2)–Os(3)	2.871(1)	C(14)–C(15)	1.41(3)
Os(2)–Os(4)	2.797(1)	C(15)–C(16)	1.37(3)
Os(3)–Os(4)	2.792(1)	C(13)–C(17)	1.50(3)
Os(4)–C(11)	2.23(2)	Os(4)–C(10)	1.90(2)
Os(4)–C(12)	2.21(2)	Os(1)–C(10)	2.35(2)
Os(4)–C(13)	2.30(2)	C(10)–O(10)	1.19(2)
Os(4)–C(14)	2.24(2)	mean Os–C_{term}	1.90(2)
Os(4)–C(15)	2.26(2)	mean C–O_{term}	1.14(2)
Os(4)–C(16)	2.28(2)		
Os(4)–C(10)–O(10)	153(1)		

p.p.e. This procedure has been shown to guarantee an exact knowledge of the immediate molecular environment.

The contributions of the Ru and Os atoms were not taken into account. A justification for this approximation has been given previously.[1,5] It is only necessary to recall that p.p.e. calculations for transition-metal clusters have no pretentions of obtaining 'true' crystal potential-energy values, rather they are used as a convenient means of investigating the molecular environment within the crystalline lattice.

In order to evaluate the potential-energy barriers to reorientation, p.p.e. values were calculated for different conformations of the arene fragments. These fragments were rotated in steps of 10° about the axes passing through the co-ordinated metal atom (in the η^6 bonding mode) or the middle of a triangular cluster face (in the μ_3 bonding mode) and the centres of the C_6 rings. Calculated positions (C–H 1.08 Å) were used for the H atoms in the aromatic ligands. Methyl groups were treated as Cl atoms centred on the C(Me) positions. This was necessary to take into account the almost free rotational motion of the Me groups in the solid and is justified by the similarity of the bulk of the Me group and Cl atom.[11]

Relative potential-energy profiles (ΔE) were calculated as ΔE = p.p.e. − p.p.e. (min.), where p.p.e. (min.) is the value corresponding to the observed structure (0° rotation). The intermolecular (ΔE_{inter}) and intramolecular (ΔE_{intra}) contributions were calculated separately; ΔE_{tot} was obtained as $\Delta E_{inter} + \Delta E_{intra}$. No co-operation or relaxation of the molecules surrounding the reorienting fragment was allowed ('static environment' approximation).[12]

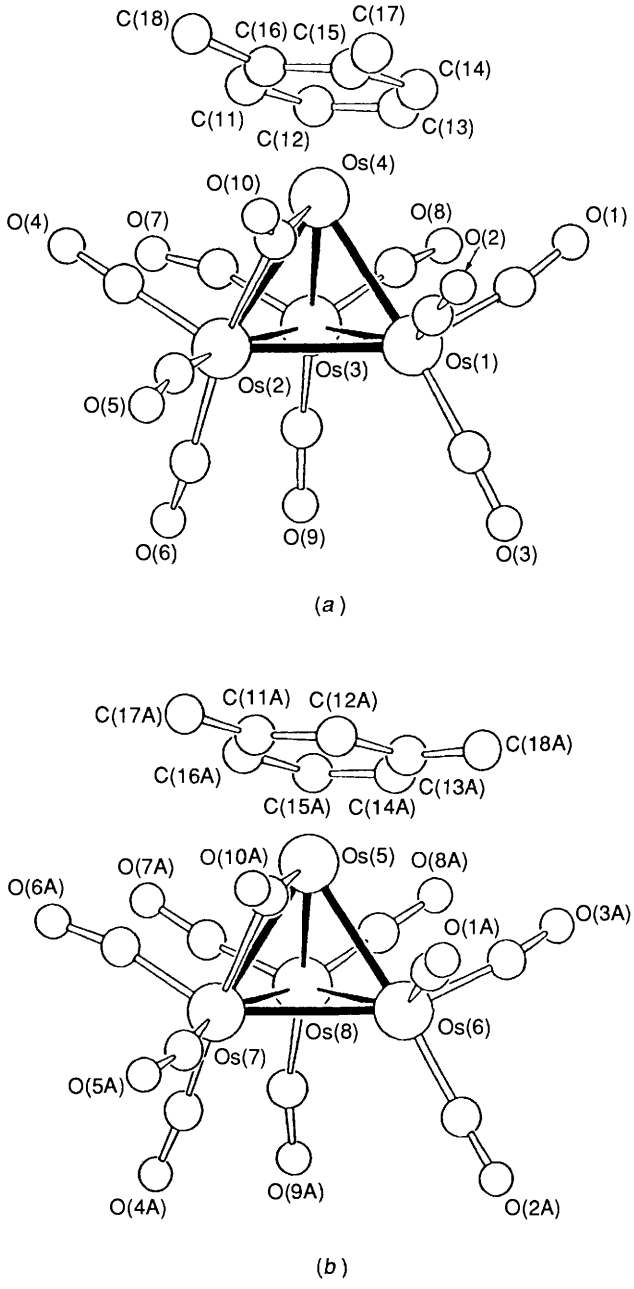

Fig. 2 The molecular structure of the two independent molecules present in crystals of compound **3**: (*a*) $C_6H_4Me_2$-*o*, (*b*) $C_6H_4Me_2$-*m*. Details as in Fig. 1

All calculations were carried out with the aid of the computer program OPEC,[13] SCHAKAL 88[14] was used for the graphical representation of the results.

Structural Characterization of Compounds 2, 3 and 5

The molecular structures of compounds **2** and **3** (Figs. 1 and 2) are closely related. Because of the presence of two independent molecules in the unit cell of **3**, the average parameters discussed in the following were calculated over equivalent sets of bonds in the two molecules. Relevant bond distances and angles for **2** are listed in Table 1, those for the two molecules of **3** in Table 2.

The metal framework of each of the two species is constituted of distorted Os_4 tetrahedra, with Os–Os distances ranging from 2.763(1) to 2.963(1) Å and from 2.755(3) to 2.966(3) Å in **2** and **3**, respectively [average 2.833(1) and 2.828(4) Å]. Compound **2**

Table 2 Relevant bond distances (Å) and angles (°) for compound **3**

Molecule 1		Molecule 2	
Os(1)–Os(2)	2.966(3)	Os(5)–Os(6)	2.794(3)
Os(1)–Os(3)	2.886(4)	Os(5)–Os(7)	2.795(3)
Os(1)–Os(4)	2.784(3)	Os(5)–Os(8)	2.800(4)
Os(2)–Os(3)	2.758(3)	Os(6)–Os(7)	2.960(3)
Os(2)–Os(4)	2.801(3)	Os(6)–Os(8)	2.863(4)
Os(3)–Os(4)	2.784(3)	Os(7)–Os(8)	2.755(3)
Os(4)–C(11)	2.28(4)	Os(5)–C(11A)	2.26(3)
Os(4)–C(12)	2.31(4)	Os(5)–C(12A)	2.28(3)
Os(4)–C(13)	2.29(4)	Os(5)–C(13A)	2.31(3)
Os(4)–C(14)	2.24(4)	Os(5)–C(14A)	2.32(3)
Os(4)–C(15)	2.21(4)	Os(5)–C(15A)	2.31(3)
Os(4)–C(16)	2.23(4)	Os(5)–C(16A)	2.28(3)
C(15)–C(17)	1.47(5)	C(11A)–C(17A)	1.45(4)
C(16)–C(18)	1.36(6)	C(13A)–C(18A)	1.44(5)
Os(4)–C(10)	1.95(10)	Os(5)–C(10A)	1.83(5)
Os(2)–C(10)	2.30(10)	Os(7)–C(10A)	2.41(6)
C(10)–O(10)	1.22(11)	C(10A)–O(11A)	1.21(7)
mean Os-C_{term}	1.93		1.92
mean C-O_{term}	1.21		1.21
mean Os-C_{ring}	2.26		2.29
Os(4)–C(10)–O(10)	143(8)	Os(5)–C(10A)–O(10A)	156(5)

Table 3 Relevant bond distances (Å) and angles (°) for compound **5**

Ru(1)–Ru(3)	2.865(1)	Ru(1)–C(12)	2.22(1)
Ru(1)–Ru(4)	2.878(1)	C(9)–C(10)	1.41(1)
Ru(2)–Ru(3)	2.905(1)	C(10)–C(11)	1.42(2)
Ru(2)–Ru(4)	2.846(1)	C(11)–C(12)	1.39(1)
Ru(3)–Ru(4)	2.961(1)	C(9)–C(13)	1.48(2)
Ru(3)–Ru(3A)	2.865(1)	C(11)–C(14)	1.50(1)
Ru(4)–Ru(4A)	2.848(1)	Ru(4)–C(8)	2.06(1)
Ru(1)–C	1.90(1)	C(8)–C(8)	1.17(2)
Ru(2)–C	2.11(1)	mean Ru–C_{term}	1.88(1)
Ru(3)–C	2.05(1)	mean C–O_{term}	1.14(2)
Ru(4)–C	2.07(1)	Ru(4) · · · C(5)	2.82
Ru(1)–C(9)	2.23(2)	C(5)–O(5)	1.14(1)
Ru(1)–C(10)	2.23(1)		
Ru(1)–C(11)	2.27(1)		
Ru(4)–C(8)–O(8)	136.2(3)	Ru(3)–C(5)–O(5)	167(1)
Ru(3)–C(5)	1.91(3)		

bears an η^6-toluene ligand co-ordinated to a tetrahedron apex; the same bonding mode is adopted by the arene in compound **3**, but, while the xylene ligand is of *meta* type in one of the two independent molecules, it is *ortho* in the second molecule. Average Os–C(ring) distances are 2.25(2) and 2.27(4) Å in **2** and **3**, respectively. Unfortunately, because the poor quality of the data, only the gross features of compound **3** were revealed; however, the structural parameters are accurate enough for the purposes of the present work.

All the values mentioned above are strictly comparable to the average Os–Os and Os–C(benzene) distances of 2.839(1) and 2.24(2) Å observed in the closely related species **1**,[7] in which a benzene ligand is η^6-co-ordinated to a metal centre in the same fashion as in **2** and **3**. Another feature shared with compound **1** is the presence of a CO ligand which is forced into a μ-semibridging position [Os(4)–C(10) 1.90(2) and Os(1)–C(10) 2.35(2) in **2**; average Os–C 1.89(10) and 2.36(10) Å in **3**], because of the spacial requirements of the arene ligands in **2** and **3**. The 'conformation' of the ring in the two independent molecules of **3** with respect to the axial CO groups and to the semibridging ligand [Fig. 2(*a*) and (*b*)] is almost identical to that observed in **2**. In both species the two H(hydride) atoms are believed to bridge the two 'long' Os–Os bonds. This is supported by the CO-ligand displacement observed around these co-ordination sites.

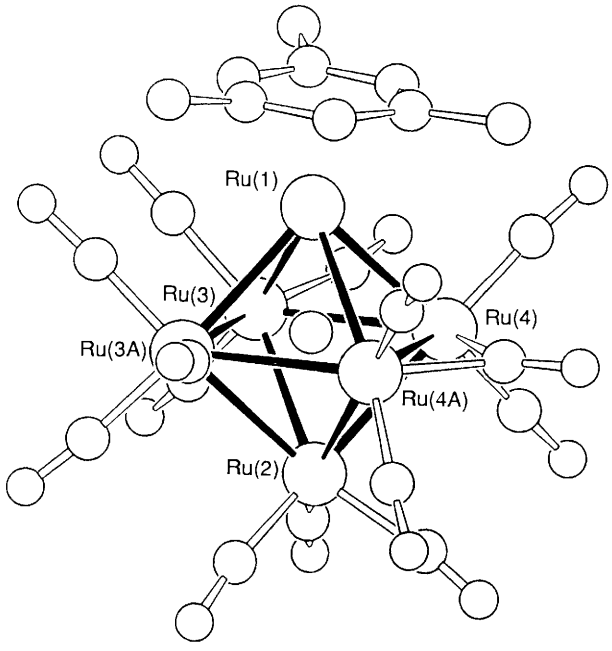

Fig. 3 The molecular structure of compound **5**; H atoms are omitted for clarity

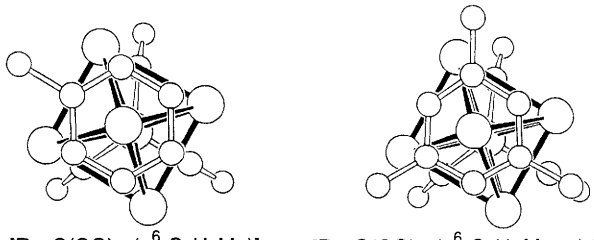

Scheme 1 Comparison between the rotameric 'conformation' of the arene ligand with respect to the opposite $(CO)_3$ unit in the structures of compounds **4** and **5**

The hexanuclear cluster **5** was the first interstitial carbido cluster characterized by X-ray diffraction.[15,16] Since the original structural data are not available, we have redetermined its solid-state structure. The updated set of relevant structural parameters for **5** is reported in Table 3. The Ru–Ru bond distances fall in the range 2.846(1)–2.961(1) [average 2.881(1) Å] in fairly good agreement with those reported earlier;[15] Ru–C(carbide) distances average 2.03(1) Å. A view of the molecule is shown in Fig. 3.

Interestingly, as previously observed in **4**,[17] the carbide atom does not lie midway between the apical Ru atom bearing the arene ligand and that which is opposite but is appreciably displaced towards the substituted Ru atom [C–Ru(1) 1.90(1), C–Ru(2) 2.11 Å]. As in **4**, there is also a weak semibridging interaction involving the terminal ligands coplanar with the bridging one [Ru(3)–C(5)–O(5) 167(1)°; Ru(3)–C(5) 1.91(1), Ru(4) · · · C(5) 2.82(1) Å]. In spite of these similarities there is a remarkable difference between the structures of **4** and **5**. As shown in Scheme 1, while the methyl group of the toluene ligand in **4** is 'staggered', the methyl groups of the mesitylene ligand in **5** are 'eclipsed' with respect to the tricarbonyl unit belonging to the opposite Ru atom. The different 'conformation' of this $(CO)_3$ unit does not break the molecular (and crystallographic) *m* symmetry of the molecule. This difference cannot be justified in terms of electronic effects, nor can it be due to *intra*molecular interactions. Its origin must be found at the *inter*molecular level, *i.e.* the two different 'conformations' are dictated by the specific packing requirements of the two molecules in the solid state (see below).

The C(arene)–C(arene) distances range from 1.39(1) to

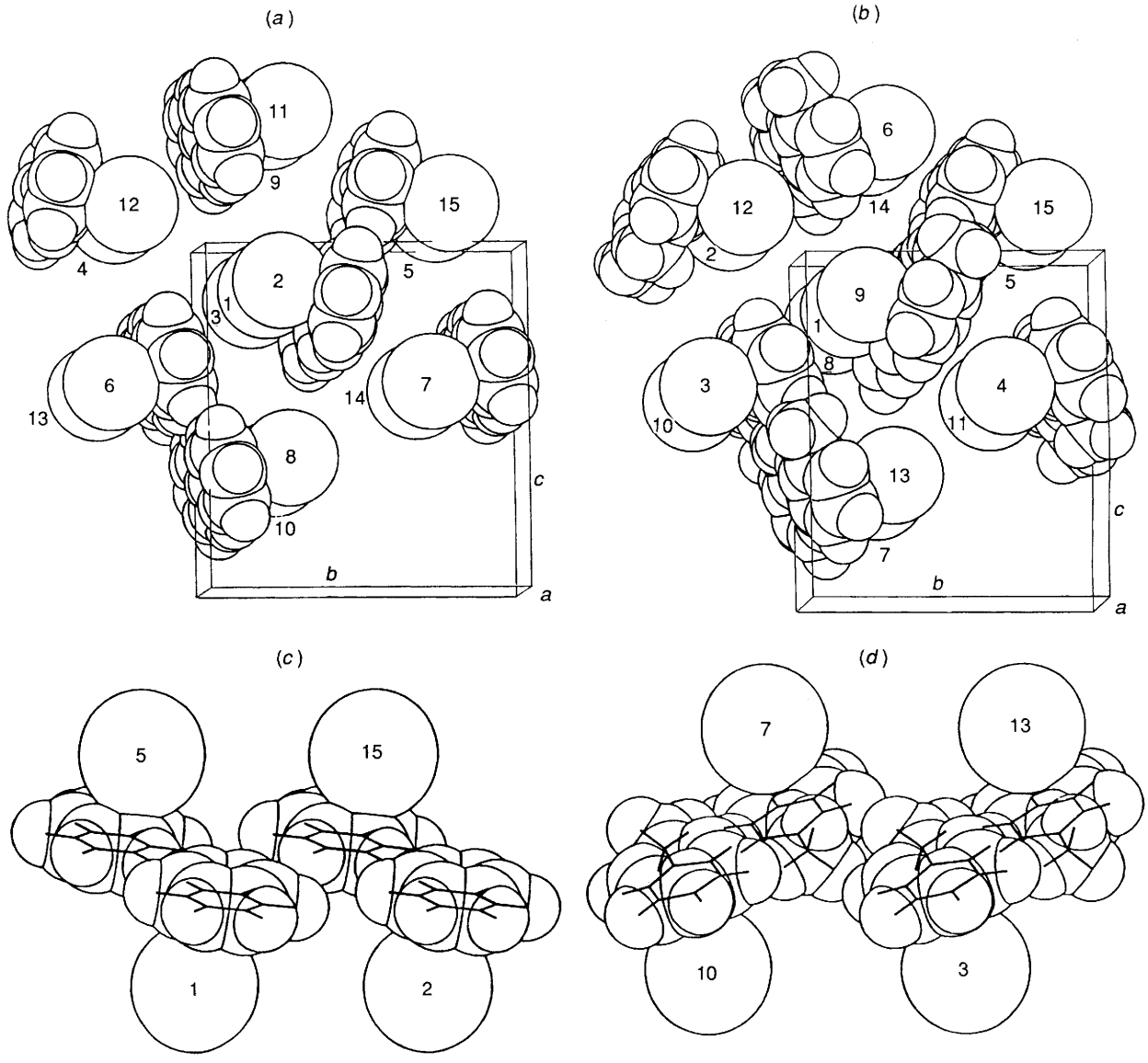

Fig. 4 Schematic representation of the molecular organization in crystals of compounds **1** (*a*) and **2** (*b*) showing the ribbon-like distribution of the arene fragments. The metal frameworks and the carbonyl ligands are omitted for clarity and represented by large spheres. The numbering corresponds to the symmetry operations which generate the FNM from the RM; unit-cell axes are also shown. The molecular packing relationship between **1** and **2** along the ribbons is shown in (*c*) and (*d*)

1.42(1) Å and their distribution does not conform to the idealized three-fold symmetry of the arene, while the two independent C(arene)–C(methyl) distances are 1.48(2) and 1.50(1) Å. The methyl groups are slightly bent above the arene plane [elevation 0.08 and 0.21 Å for C(13) and C(14), respectively].

Molecular Organization in Crystals of Compounds 1–3

The reference molecules (RMs) of both compounds **1** and **2** are surrounded by 14 FNM [Fig. 4(*a*) and (*b*)]. These 14 molecules account for 95.9 and 96.4% of the total p.p.e., in **1** and **2**, respectively. It is apparent, from Fig. 4(*a*) and (*b*), that in spite of the structural difference due to the presence of a toluene ligand rather than benzene, the mode of packing in solid **1** and **2** is nearly the same. The arene ligands form ribbons throughout the crystal lattice. The ribbons are generated by the interlocking of two rows of arene fragments in a chevron-like fashion [Fig. 4(*c*) and (*d*)]. It is significant that this pattern is retained on substituting toluene for benzene. The methyl groups are inserted in between pairs of ligands belonging to the same ribbon. The main consequence of this insertion is the lengthening of the unit-cell *a* axis from 8.209 to 9.118 Å on passing from **1** to **2**, while the overall separation between parallel ribbons along the *b* axis decreases from 15.029 to 13.957 Å and that along the *c* axis is almost unaffected (16.453 in **1** and 16.567 Å in **2**, Fig. 4).

Moreover, the RM in both **1** and **2** interacts directly with a second molecule related by a crystallographic inversion centre. This interaction, however, is not equivalent in **1** and **2**: its *relative* contribution to the p.p.e. is larger in **2** than in **1** (−11.5 and −7.0 kcal mol^{-1}). On the other hand the intermolecular interaction along the ribbons (translation along the *a* axis) is less relevant in **2** than in **1** (−5.3 and −7.3 kcal mol^{-1}). This difference seems to indicate that the more efficient CO interlocking in **2** 'compensates' for the loss in intermolecular cohesion consequent upon the increase in intermolecular separation along the ribbons on passing from **1** to **2**.

The presence of two independent molecules within the lattice makes any rationalization of the packing modes in crystals of compound **3** difficult. The *ortho* and *meta* positioning of the methyl groups over the ligands is no longer compatible with the ribbon-like distribution of the arenes seen in **1** and **2**.

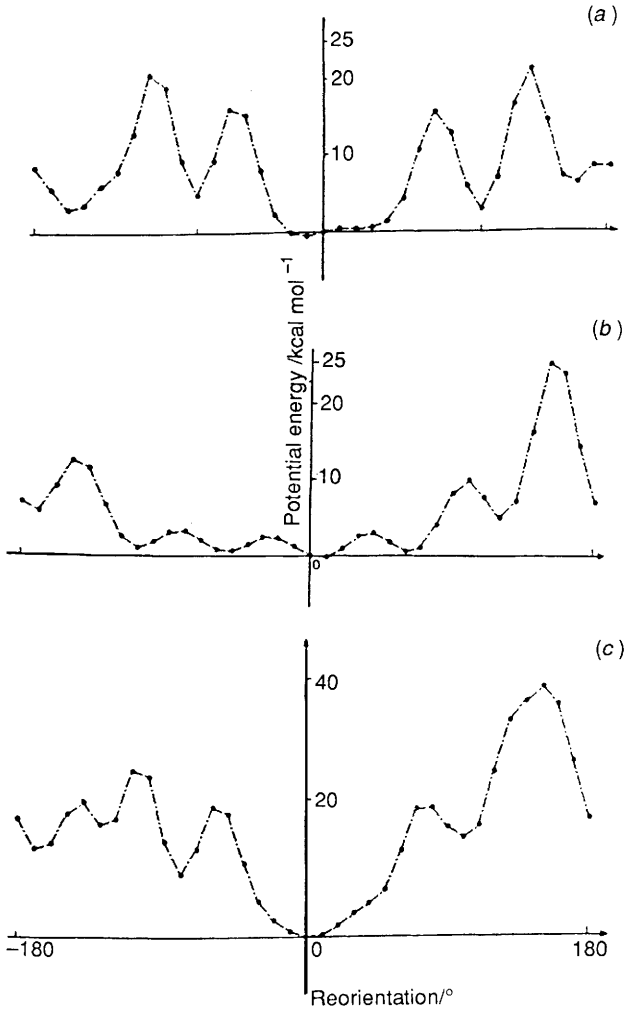

Fig. 5 Potential-energy profiles of ΔE_{inter} (*a*), ΔE_{intra} (*b*), and ΔE_{tot} (*c*) for reorientation of the toluene ligand in compound **2** around its co-ordination axis

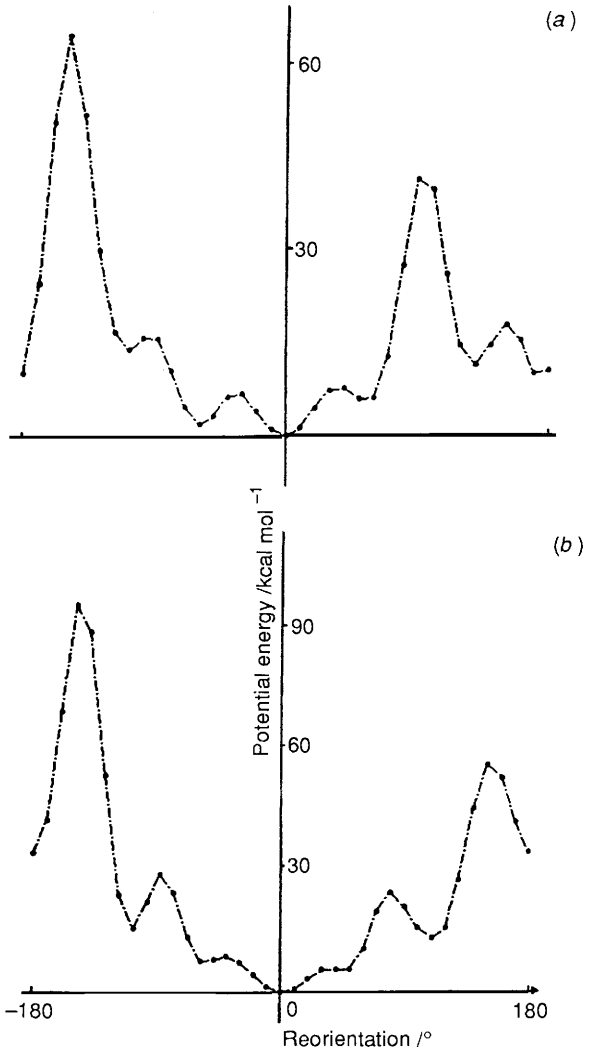

Fig. 6 Potential-energy profiles ΔE_{tot} for reorientation of the *meta*- (*a*) and *ortho*-xylene (*b*) ligands in compound **3**

Reorientational Motion in Compounds 1–3

The intermolecular barrier to reorientation in compound **1** (ΔE_{inter}) is *ca.* 5.9 kcal mol^{-1} with minima of equivalent energy every 60° 'hop' of the C atom from one position to the next; ΔE_{intra} also shows a sinusoidal behaviour, in-phase with ΔE_{inter}, with maxima of *ca.* 3.0 kcal mol^{-1}; thus ΔE_{tot} (the sum of ΔE_{inter} and ΔE_{intra}) retains the $\pi/6$ aspect with a maximum value of *ca.* 9.0 kcal mol^{-1}. This is by far the largest reorientational barrier to rotation of an η^6-co-ordinated benzene fragment observed in arene clusters. The values of ΔE_{inter}, ΔE_{intra}, and ΔE_{tot} can be compared with those previously reported for $[Os_3(CO)_7(\mu_3\text{-}\sigma\text{:}\eta^2\text{:}\sigma\text{-}C_2Me_2)(\eta^6\text{-}C_6H_6)]$[5b] [2.0, 1.8 (not 'in-phase' with ΔE_{inter}), 2.2 kcal mol^{-1}] and for the mononuclear complexes $[M(CO)_3(\eta^6\text{-}C_6H_6)]$ (M = Cr or Mo)[2b] (at room temperature ΔE_{tot} = 4.7 and 5.9 kcal mol^{-1} for Cr and Mo, respectively) and $[Cr(C_6H_6)_2]$ (at room temperature 2.9 kcal mol^{-1}). The values of the p.p.e. barrier for these latter mononuclear complexes were in substantial agreement with the potential barrier/activation energies obtained by various spectroscopic methods.[3]

Complete reorientation of the toluene ligand in compound **2** appears to be prevented by the upsurge in the high potential-energy barrier (see Fig. 5). The profile of ΔE_{inter} is characterized by a rather large and flat bottom (< 10 kcal mol^{-1} between −40 and +50° rotation) surrounded by two maxima of *ca.* 18 kcal mol^{-1}; 'local' minima (*ca.* 3 and 5 kcal mol^{-1}) are seen after rotation of +100 or −80°, respectively; ΔE_{intra} shows two large maxima after ±150° rotation due to 'clashes' between the methyl group and the radial ligands C(5)O(5) and C(6)O(6) and, to a smaller extent, the semibridging ligand C(10)O(10). The resulting total profile (ΔE_{tot}) shows that the toluene ligand in **2** sits in a large p.e. well, while a barrier of *ca.* 36 kcal mol^{-1} prevents complete reorientation. This behaviour is in agreement with that observed in the mononuclear complexes $[M(CO)_3(C_6H_5Me)]$ (M = Cr or Mo) where full-scale reorientation (but not large-amplitude motion) is similarly forbidden.[2b,f] Similarly, reorientation of both arene ligands in compound **3** is forbidden at room temperature as clearly shown in Fig. 6(*a*) and (*b*). The *intramolecular* locking of the *o*- and *m*-$C_6H_4Me_2$ ligands is very tight (ΔE_{intra} 85 and 60 kcal mol^{-1}, respectively), so that the total reorientational barriers in **2** and **3** are essentially determined at the intramolecular level.

It should be stressed, however, that our calculations do not allow for co-operative motions of the ligands belonging to the same molecule or to the surrounding ones. It may well be that small concerted displacements of the arene ligands and/or of the CO groups might suffice in lowering the reorientational barrier to some extent.

Molecular Organization in Crystalline Compounds 4–6

Fig. 7(*a*) and (*b*) shows that there are 14 FNM around the RM in compound **4** and 12 in **5**. It is interesting that only this latter species, of the several examined in this study, adopts the typical anticuboctahedral arrangements observed in transition-metal binary carbonyls with 12 FNM[1a] While the arene fragments form layers in the lattice of **5**, the distribution in **4** is quite similar

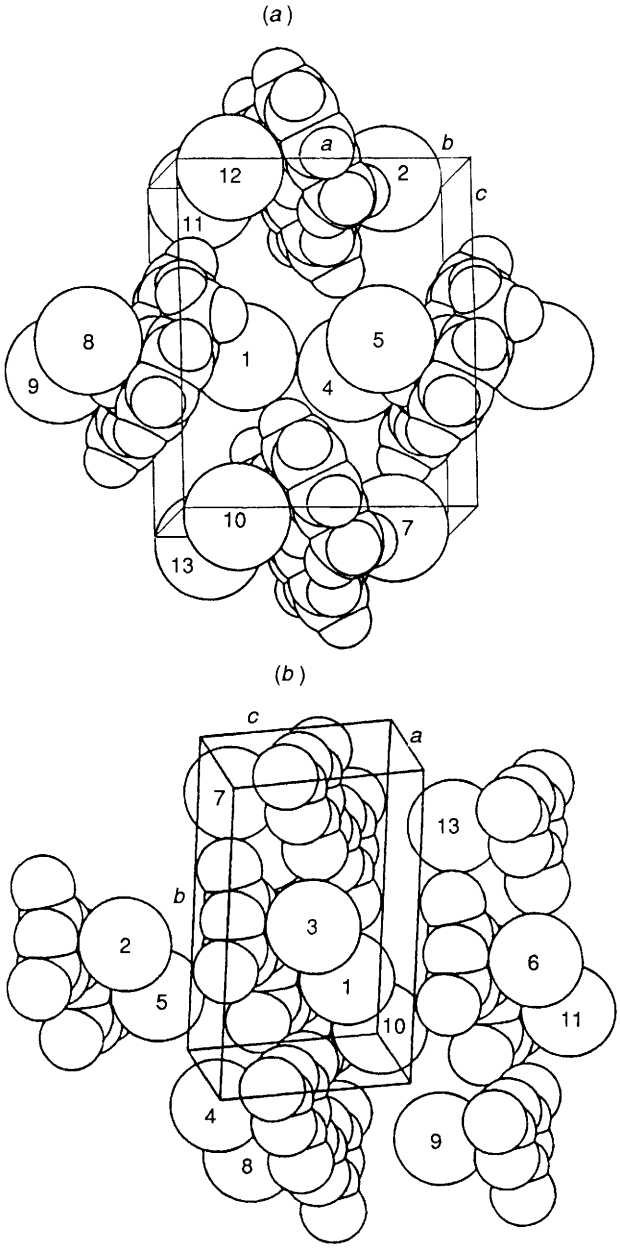

Fig. 7 Schematic representation of the molecular organization in crystals of compounds **4** (*a*) and **5** (*b*) showing the ribbon-like distribution of the arene fragments. The metal framework and the carbonyl ligands are omitted for clarity and represented by large spheres. The numbering corresponds to the symmetry operations which generate the FNM from the RM; unit-cell axes are also shown

to that observed above in **1** and **2**, *i.e.* in spite of the rather different molecular geometry and of the different size of the molecules, the ribbon-like pattern established by the aromatic ligands is maintained in **4**. The distribution of the arene ribbons in the lattice of **1**, **2** and **4** recalls the 'herring-bone' pattern seen in the crystal packing of most fused-ring hydrocarbons.[18] The relationship between next-neighbouring molecules in **4** and **5** is very similar to that observed in **1** and **2**.

The molecule $[Ru_6C(CO)_{11}(\mu_3\text{-}\eta^2\text{:}\eta^2\text{:}\eta^2\text{-}C_6H_6)(\eta^6\text{-}C_6H_6)]$ **6** is unique among the arene clusters characterized to date, in that it contains two different benzene fragments. It crystallizes in the triclinic space group $P\bar{1}$, with one independent molecule in the asymmetric unit.[19]

In order to decode the packing pattern let us focus first on the molecular structure: the two benzene ligands occupy an apical (η^6 bonding mode) and a facial site (μ_3 bonding mode) over the Ru_6 framework, respectively (see Fig. 8). The angle between the

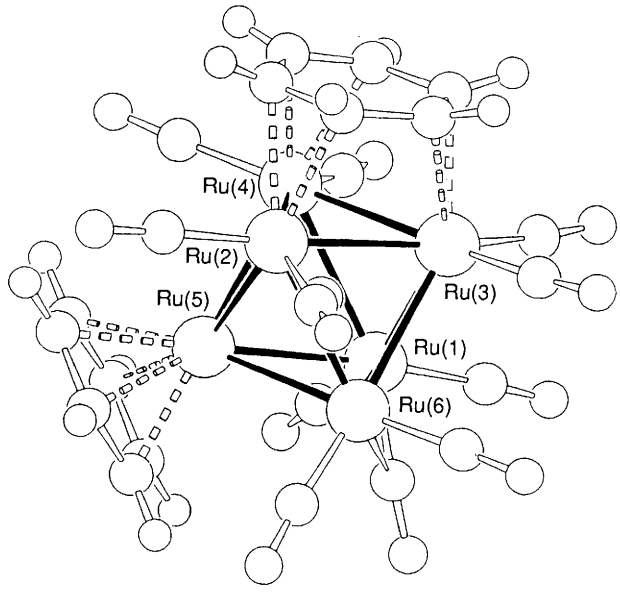

Fig. 8 The molecular structure of compound **6** from ref. 19

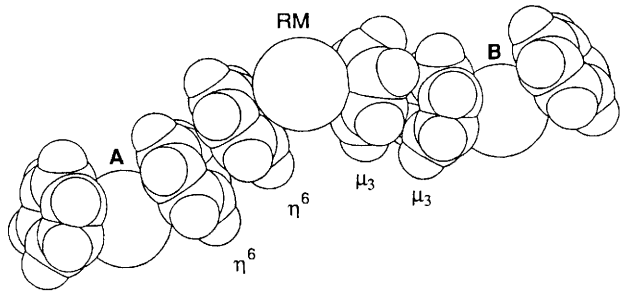

Fig. 9 Schematic view of the intermolecular interactions in crystals of compound **6**. The RM is 'linked' to molecule **A** *via* $\eta^6\eta^6$-benzene coupling, and to molecule **B** *via* $\mu_3\mu_3$-benzene coupling. For sake of clarity the entire cluster body (metal core and CO ligands) is represented by large spheres

two ring planes is *ca.* 53°; this is a key feature for the understanding of the crystal packing. Again, there are 14 FNM around the RM in **6** accounting for *ca.* 99.5% of the total p.p.e. These molecules do not form a close-packed arrangement. There is a remarkable interaction between the RM and two next-neighbouring molecules referred to the RM by the crystallographic centres of symmetry. These molecules are placed with their benzene ligands almost face-to-face with respect to those belonging to the RM, as shown in Fig. 9. The arene–arene sequence is $\eta^6\eta^6$–$\mu_3\mu_3$–$\eta^6\eta^6$–$\mu_3\mu_3$, *etc.*, thus the RM has its apical benzene interacting with the apical benzene of molecule **A** and its μ_3-benzene interacting with the μ_3-benzene of molecule **B**. The inter-ring separation is slightly longer in the $\eta^6\eta^6$ pair (distance between planes 3.56 Å) than in the $\mu_3\mu_3$ pair (3.29 Å), this latter separation being slightly smaller than in graphite itself. Interestingly the ring pairs are not exactly superposed (*i.e.* with eclipsed C atoms) but are shifted in a typical graphitic-like pattern as shown in Scheme 2 ($\eta^6\eta^6$ shift 1.09 Å, $\mu_3\mu_3$ shift 1.44 Å). This pattern of molecular coupling leads to the formation of infinite 'snake-like' chains of arene–arene joint molecules through the crystal lattice as depicted in Fig. 10. The chains extend in the 011 direction in the triclinic cell. The snake-to-snake interaction is based on CO–CO interlocking between neighbouring molecules separated by translation along the *a* axis.

Arene Reorientation in Compounds 4–6

The similarity between the toluene species **2** and **4** is also apparent from the dynamic behaviour of the toluene ligand. As

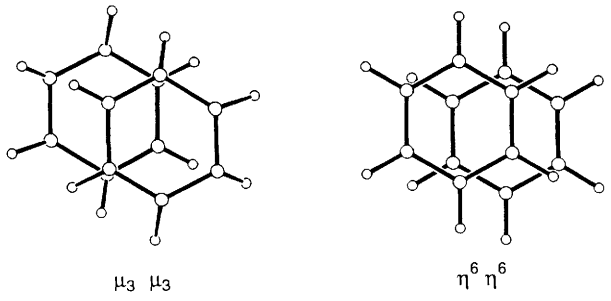

Scheme 2 Projections perpendicular to the $\eta^6\eta^6$ and $\mu_3\mu_3$ pairs of benzene fragments in crystalline compound **6** showing the graphite-like interactions

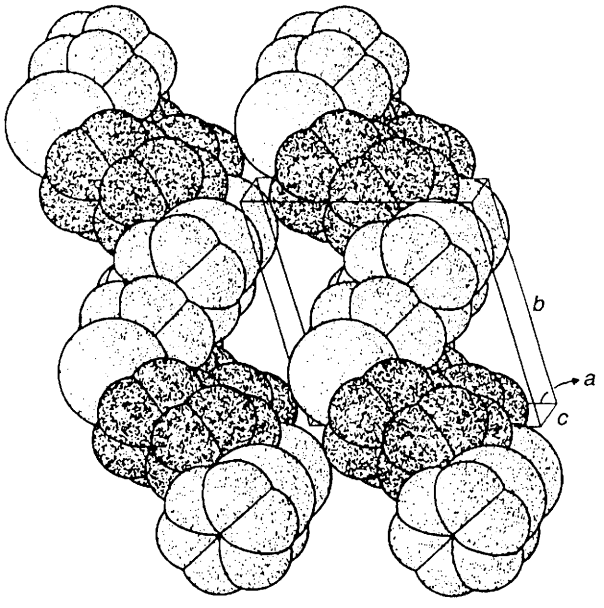

Fig. 10 The organization of the 'snake-like' molecular rows within the crystal lattice of compound **6**. The rows extend along the 011 direction in the triclinic cell. Hydrogen atoms are omitted for clarity

shown in Fig. 11 complete reorientation of the toluene ligand around its co-ordination axis is hindered by intermolecular interactions and restricted by intramolecular ones.

As expected arene reorientation is completely restricted in compound **5**. Both ΔE_{inter} and ΔE_{intra} show a sinusoidal behaviour with large potential-energy barriers centred at ± 60 and $\pm 180°$ in accord with the three-fold symmetry of the fragment. The groups opposing the intramolecular motion are the same as in **4**, while the intermolecular barrier is mainly determined by the interaction of the arene fragment with an apical $(CO)_3$ group of a neighbouring molecule. The resulting total barrier (see Fig. 12) is rather large (ΔE_{tot} *ca.* 55 kcal mol^{-1}). This behaviour is in agreement with that observed in crystals of the mononuclear complex $[Mo(CO)_3(C_6H_3Me_3)]$.[20]

Both benzene ligands in compound **6** appear to be able to undergo a rotational jumping motion in the solid state. Their behaviour, however, is not identical. In the case of the η^6 ligand, ΔE_{inter} and ΔE_{intra} are low (maximum 1.6 and 1.2 kcal mol^{-1} respectively) and 'in-phase', *i.e.* minima and maxima correspond almost precisely, yielding a ΔE_{tot} barrier of *ca.* 2.8 kcal mol^{-1} [see Fig. 13(*a*)]. The μ_3 ligand presents higher potential barriers to reorientation [ΔE_{inter}(max.) 4.6, ΔE_{intra}(max.) 4.6 kcal mol^{-1}]. The minima and maxima are, however, not in phase, thus resulting in a rather flat ΔE_{tot} profile with a maximum value of *ca.* 4.8 kcal mol^{-1} [see Fig. 13(*b*)]. It is also noteworthy that the rotameric position of the μ_3 ligand is close to a maximum in the intramolecular potential. This indicates that the situation dictated by the Ru_3-C_6H_6 bonding interaction is slightly repulsive in terms of intraligand non-bonding.

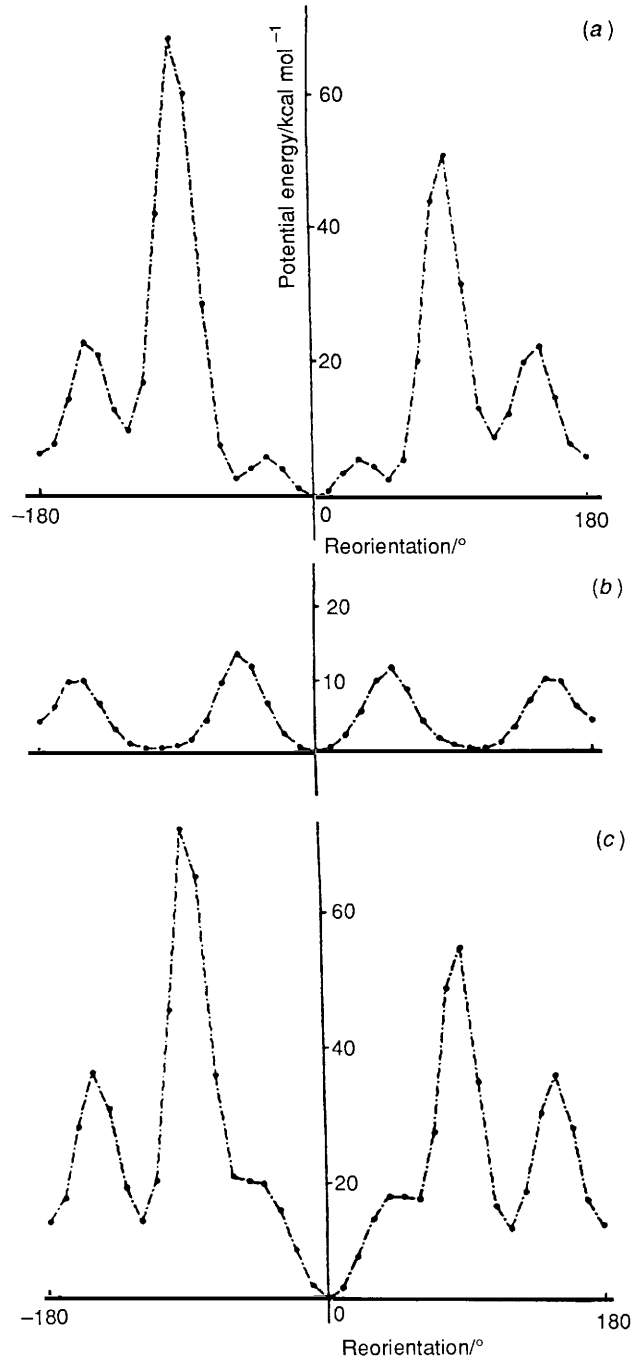

Fig. 11 Potential-energy profiles ΔE_{inter} (*a*), ΔE_{intra} (*b*), and ΔE_{tot} (*c*) for reorientation of the toluene ligand in compound **4** around its co-ordination axis

A similar picture of the balance between bonding and non-bonding interactions had been previously seen in the structure of $[Ru_3(CO)_9(\mu_3\text{-}\eta^2\text{:}\eta^2\text{:}\eta^2\text{-}C_6H_6)]$,[5a] which also contains a face-capping benzene fragment. The reorientational barriers in crystals of this species are strictly comparable with those of **1** (ΔE_{inter} 3.9, 5.0; ΔE_{intra} 4.0, 4.0; ΔE_{tot} 4.5, 6.3 kcal mol^{-1}, at room temperature and 193 K respectively). In both compounds, in spite of the differences in structure and cluster nuclearity, the μ_3-benzene fragment lies on a 'bed' of three Ru atoms belted by six 'radial CO' groups.

The η^6 ligand in compound **6**, on the contrary, is much further away from the four surrounding CO ligands so that intramolecular repulsions are less relevant. This results in a relatively low ΔE_{tot} barrier, thus accounting for the positional disorder observed in the structural model.[19]

Considering the packing relationship described in the

Table 4 Crystal data and details of measurements for compounds **2**, **3** and **5**[a]

	2	**3**	**5**
Formula	$C_{17}H_{10}O_{10}Os_4$	$C_{18}H_{12}O_{10}Os_4$	$C_{24}H_{12}O_{14}Ru_6$
M_r	1135.04	1149.07	1134.52
Crystal size (mm)	0.10 × 0.12 × 0.12	0.15 × 0.10 × 0.12	0.14 × 0.12 × 0.15
System	Monoclinic	Orthorhombic	Monoclinic
Space group	$P2_1/n$	$Pbca$	$P2_1/m$
a/Å	9.118(2)	21.719(8)	9.468(7)
b/Å	13.957(4)	13.396(7)	15.835(7)
c/Å	16.567(7)	31.253(6)	10.566(3)
β/°	96.67(3)	—	110.36(4)
U/Å^3	2094	9093	1485
Z	4	16	2
F(000)	1984	8064	1064
D_c/g cm^{-3}	3.60	3.36	2.54
μ(Mo-Kα)/cm^{-1}	233.0	223.6	27.6
ω-Scan width/°	1.10	1.20	1.50
Requested counting $\sigma(I)/I$	0.02	0.02	0.01
Prescan rate/° min^{-1}	8	5	5
Maximum scan time/s	100	100	120
Octants explored	$\pm h, +k, +l$	$+h, +k, +l$	$\pm h, +k, +l$
Measured reflections	3624	8015	2880
Unique observed reflections used in the refinement	3041 $[F_o > 4\sigma(F_o)]$	2832 $[F_o > 6\sigma(F_o)]$	1881 $[F_o > 4\sigma(F_o)]$
No. of refined parameters	282	268	216
Absorption correction (min.,max.)[b]	0.53, 1.00	0.27, 1.00	—
R, R'[c]	0.047, 0.049	0.076, 0.078	0.049, 0.052
S	0.83	2.97	0.76
K, g	0.99 0.006	2.54, 0.002	0.82 0.005

[a] Details in common: λ(Mo-Kα) = 0.710 69 Å, θ range 2.5–25°; scan mode ω–2θ; prescan acceptance $\sigma(I)/I = 0.5$. [b] Applied by the Walker and Stuart method.[21b] [c] $R' = \Sigma[(F_o - F_c)w^{\frac{1}{2}}]/\Sigma F_o w^{\frac{1}{2}}$, where $w = K/[\sigma^2(F) + |g|F^2]$.

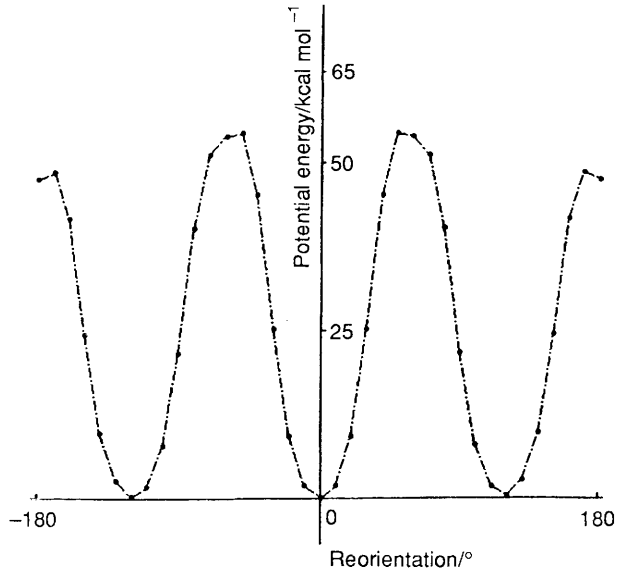

Fig. 12 Potential-energy profiles ΔE_{tot} for reorientation of the mesitylene ligand in compound **5**

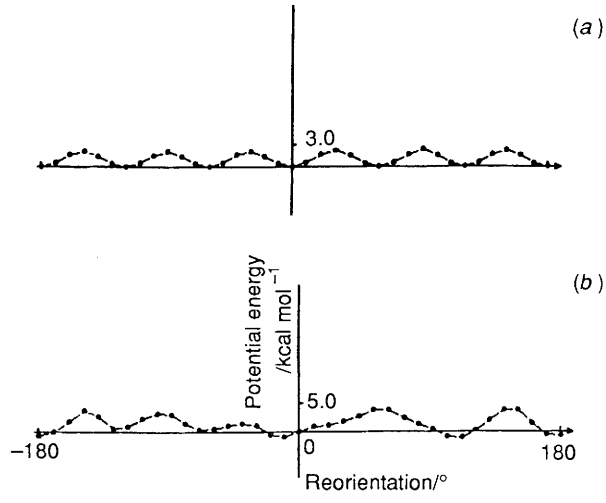

Fig. 13 Potential-energy profiles ΔE_{tot} for reorientation of the η^6-benzene ligand (*a*) and of the μ_3-benzene ligand (*b*) in compound **6**

previous section, a sort of paired rotational motion can be envisaged for the benzene ligands facing each other along the molecular 'snake'. This might cause a substantial decrease in the reorientational barriers. It is fascinating to regard the crystal of **6** as constituted of long chains of molecules held together by sets of interacting rotating wheels.

Conclusion

We have demonstrated that, in spite of the differences in molecular complexity (nuclearity of the metal cluster, number of ligands, shape of the metal-atom polyhedron) and in crystal features (site and space-group symmetry), precise relationships can be found between the packing modes of high-nuclearity arene clusters of Ru and Os. Our observations can be summarized as follows.

(*i*) There is a clear tendency to group the arene fragments in ribbons or layers through the crystal lattice. This is most certainly due to the difficulty (in terms of intermolecular interlocking) of intermixing flat fragments with the cavities and bumps of the carbonyl coverage. The crystallization process copes with this problem by grouping together the arene fragments thus preserving optimum CO • • • CO interlocking for the remaining parts of the molecules. This effect is particularly relevant in compound **6**, which contains two arene fragments, resulting in the sophisticated pattern discussed above.

(*ii*) The study of the reorientational barriers lends further support to the general idea that disk-like benzene fragments, whether bound to the metal frame in facial or terminal mode,

cannot easily be 'locked in' by the surrounding ligands in the molecules or by the surrounding molecules in the lattice.

(*iii*) On the contrary, ligands with protruding groups (toluene, xylene, mesitylene, *etc.*) invariably exhibit highly restricted motion. At most, these ligands can execute large-amplitude librations at the bottom of flat p.e. wells.

(*iv*) The intramolecular interlocking of these ligands has also been shown to be very effective in preventing reorientational freedom.

The understanding of the way in which complex molecules of

Table 5 Fractional atomic coordinates for compound **2**

Atom	*x*	*y*	*z*
Os(1)	−0.055 79(6)	0.173 97(4)	0.931 97(3)
Os(2)	0.250 37(5)	0.133 65(4)	0.898 51(3)
Os(3)	0.007 93(6)	0.158 98(4)	0.773 43(3)
Os(4)	0.120 59(6)	0.313 61(4)	0.868 05(3)
C(1)	−0.161 3(18)	0.062 6(11)	0.897 8(9)
O(1)	−0.235 6(16)	−0.003 8(9)	0.880 4(8)
C(2)	−0.231 6(16)	0.251 3(12)	0.919 0(10)
O(2)	−0.329 6(14)	0.297 0(9)	0.905 7(10)
C(3)	−0.060 1(16)	0.162 1(11)	1.045 5(8)
O(3)	−0.061 7(15)	0.151 5(11)	1.116 9(8)
C(4)	0.324 7(15)	0.010 2(12)	0.929 6(8)
O(4)	0.371 6(13)	−0.063 4(7)	0.948 9(8)
C(5)	0.354 9(16)	0.197 3(13)	0.989 7(11)
O(5)	0.414 4(16)	0.237 5(10)	1.042 1(9)
C(6)	0.398 2(16)	0.158 7(12)	0.827 4(9)
O(6)	0.483 1(16)	0.168 2(12)	0.784 5(9)
C(7)	−0.083 8(16)	0.048 0(14)	0.730 4(8)
O(7)	−0.142 1(17)	−0.022 3(11)	0.701 1(8)
C(8)	−0.154 5(17)	0.238 4(11)	0.733 3(9)
O(8)	−0.252 0(14)	0.284 9(11)	0.710 7(9)
C(9)	0.122 1(18)	0.178 1(11)	0.687 1(10)
O(9)	0.190 1(16)	0.186 4(9)	0.634 1(8)
C(10)	0.082 1(17)	0.309 8(12)	0.978 2(9)
O(10)	0.093 6(17)	0.338 9(9)	1.046 0(7)
C(11)	0.260 8(23)	0.371 2(13)	0.777 7(14)
C(12)	0.315 7(18)	0.404 7(12)	0.856 3(10)
C(13)	0.227 3(22)	0.460 2(12)	0.898 6(11)
C(14)	0.073 3(19)	0.471 2(12)	0.868 3(11)
C(15)	0.017 3(21)	0.435 6(12)	0.791 3(13)
C(16)	0.113 7(25)	0.390 5(12)	0.746 6(12)
C(17)	0.280 9(27)	0.503 1(14)	0.980 0(13)

Table 7 Fractional atomic coordinates for compound **5**

Atom	*x*	*y*	*z*
Ru(1)	0.296 07(13)	0.25	0.569 62(12)
Ru(2)	0.431 61(16)	0.25	0.974 00(14)
Ru(3)	0.202 09(11)	0.159 55(6)	0.761 32(10)
Ru(4)	0.521 99(10)	0.160 07(6)	0.781 77(9)
C	0.355 2(17)	0.25	0.759 2(17)
C(1)	0.650 8(27)	0.25	1.084 4(26)
O(1)	0.762 3(18)	0.25	1.153 0(20)
C(2)	0.393 5(23)	0.159 8(10)	1.076 9(16)
O(2)	0.385 6(20)	0.107 6(9)	1.148 8(12)
C(3)	0.108 9(17)	0.127 1(13)	0.885 9(20)
O(3)	0.043 7(16)	0.104 0(13)	0.953 8(17)
C(4)	0.016 7(16)	0.155 1(9)	0.623 3(15)
O(4)	−0.102 3(11)	0.149 2(8)	0.541 2(12)
C(5)	0.275 0(18)	0.052 6(10)	0.735 1(16)
O(5)	0.293 2(14)	−0.018 7(8)	0.708 4(15)
C(6)	0.648 6(18)	0.096 1(10)	0.925 0(14)
O(6)	0.730 2(17)	0.057 9(9)	1.010 9(13)
C(7)	0.579 0(15)	0.092 9(8)	0.661 3(14)
O(7)	0.622 7(13)	0.048 3(7)	0.598 8(12)
C(8)	0.683 4(20)	0.25	0.792 6(18)
O(8)	0.810 2(13)	0.25	0.798 3(16)
C(9)	0.407 5(23)	0.25	0.417 0(17)
O(10)	0.330 7(14)	0.173 8(9)	0.406 3(12)
C(11)	0.176 1(14)	0.172 5(9)	0.383 7(13)
C(12)	0.109 4(18)	0.25	0.376 9(17)
C(13)	0.572 0(20)	0.25	0.432 2(21)
C(14)	0.093 4(18)	0.090 3(10)	0.353 1(19)

Table 6 Fractional atomic coordinates for compound **3**

Atom	*x*	*y*	*z*
Os(1)	0.857 27(9)	0.123 48(16)	0.460 45(8)
Os(2)	0.955 01(9)	0.186 32(17)	0.521 00(8)
Os(3)	0.836 14(10)	0.161 61(18)	0.550 15(8)
Os(4)	0.862 08(10)	0.316 31(17)	0.493 47(8)
Os(5)	0.587 21(10)	0.160 80(18)	0.727 58(9)
Os(6)	0.712 61(9)	0.131 56(17)	0.712 03(8)
Os(7)	0.644 51(10)	0.012 49(17)	0.776 26(9)
Os(8)	0.671 15(11)	0.210 11(17)	0.792 19(9)
C(1)	0.774 4(10)	0.147 6(37)	0.441 5(19)
O(1)	0.723 0(7)	0.174 4(27)	0.433 0(12)
C(2)	0.894 1(18)	0.165 0(40)	0.407 4(8)
O(2)	0.905 7(19)	0.196 6(34)	0.372 2(7)
C(3)	0.865 0(63)	−0.007 3(21)	0.435 0(26)
O(3)	0.861 4(19)	−0.096 0(13)	0.427 9(15)
C(4)	0.980 5(22)	0.288 9(34)	0.560 4(13)
O(4)	0.985 6(21)	0.346 4(30)	0.590 0(12)
C(5)	1.035 1(10)	0.190 4(31)	0.494 6(15)
O(5)	1.085 5(10)	0.174 0(35)	0.480 1(16)
C(6)	0.972 9(22)	0.068 9(25)	0.554 7(13)
O(6)	0.975 0(25)	0.007 1(28)	0.582 9(14)
C(7)	0.845 1(33)	0.248 2(40)	0.599 1(14)
O(7)	0.860 5(24)	0.283 3(35)	0.633 2(10)
C(8)	0.748 7(5)	0.185 8(40)	0.548 0(17)
O(8)	0.693 8(5)	0.186 3(35)	0.554 4(16)
C(9)	0.830 0(26)	0.043 3(23)	0.585 2(16)
O(9)	0.835 2(23)	−0.041 3(21)	0.598 4(16)
C(10)	0.942 7(44)	0.300 6(82)	0.466 8(18)
O(10)	0.978 5(20)	0.340 3(33)	0.441 9(17)
C(11)	0.848 0(17)	0.456 8(31)	0.533 7(10)
C(12)	0.793 0(17)	0.403 2(31)	0.535 7(10)
C(13)	0.763 2(17)	0.375 0(31)	0.498 1(10)
C(14)	0.788 4(17)	0.400 3(31)	0.458 5(10)
C(15)	0.843 4(17)	0.453 8(31)	0.456 5(10)
C(17)	0.870 5(17)	0.476 1(31)	0.414 4(10)
C(16)	0.873 2(17)	0.482 1(31)	0.494 1(10)
C(18)	0.918 4(17)	0.547 9(31)	0.504 1(10)
C(1A)	0.689 6(30)	0.070 6(37)	0.658 8(11)
O(1A)	0.681 1(25)	0.017 9(36)	0.628 0(11)
C(2A)	0.800 6(6)	0.114 7(46)	0.708 5(20)
O(2A)	0.851 9(7)	0.088 4(36)	0.698 6(16)
C(3A)	0.722 2(27)	0.254 4(16)	0.680 4(13)
O(3A)	0.723 8(19)	0.342 8(14)	0.672 2(13)
C(4A)	0.698 8(18)	−0.002 4(31)	0.824 3(10)
O(4A)	0.730 9(17)	−0.027 3(32)	0.853 8(10)
C(5A)	0.647 9(37)	−0.123 6(14)	0.756 4(20)
O(5A)	0.643 2(23)	−0.213 6(11)	0.754 5(17)
C(6A)	0.568 9(14)	0.003 2(58)	0.808 0(15)
O(6A)	0.529 3(15)	−0.010 2(43)	0.834 5(14)
C(7A)	0.611 4(16)	0.222 5(45)	0.837 3(12)
O(7A)	0.565 8(17)	0.220 4(46)	0.859 4(14)
C(8A)	0.672 2(25)	0.352 5(9)	0.784 6(15)
O(8A)	0.672 5(21)	0.437 4(11)	0.771 8(15)
C(9A)	0.735 1(15)	0.206 5(48)	0.834 8(11)
O(9A)	0.783 8(20)	0.201 2(76)	0.853 4(19)
C(10A)	0.584 5(26)	0.029 1(36)	0.711 8(20)
O(10A)	0.568 7(15)	−0.042 1(27)	0.690 8(13)
C(11A)	0.484 3(12)	0.169 0(22)	0.717 4(12)
C(17A)	0.440 8(12)	0.087 3(22)	0.721 1(12)
C(12A)	0.512 2(12)	0.189 2(22)	0.678 2(12)
C(13A)	0.554 0(12)	0.267 8(22)	0.674 6(12)
C(14A)	0.567 8(12)	0.326 3(22)	0.710 3(12)
C(15A)	0.539 8(12)	0.306 1(22)	0.749 5(12)
C(16A)	0.498 1(12)	0.227 5(22)	0.753 1(12)
C(18A)	0.575 4(12)	0.276 1(22)	0.631 3(12)

the kind discussed herein self-assemble in the crystal lattice is expected to be of paramount importance in any attempt at appreciation of the physical and chemical properties of organometallic solids.

Experimental

X-Ray Structural Determination of Compounds **2**, **3** *and* **5**.—Crystal data and details of measurements for compounds **2**, **3** and **5** are summarized in Table 4. Diffraction intensities were collected at room temperature on an Enraf-Nonius CAD-4 diffractometer equipped with Mo-Kα radiation, and reduced to F_o. No correction for decay was necessary. The structures were solved by direct methods, which afforded the position of the metal atoms; all remaining atoms were located by subsequent Fourier difference syntheses. An absorption correction was applied to **2** and **3** by the Walker and Stuart[21b] method once the structural models were completely defined and all atoms refined isotropically. The structural model refinement was made by least-squares calculations, the function minimized being $\Sigma w(F_o - KF_c)^2$. The weighting scheme employed was $w = K/[\sigma^2(F) + |g|F^2]$ where both K and g were recalculated after each cycle of least-squares refinement. For all calculations the SHELX 76[21a] package of crystallographic programs was used with analytical scattering factors, corrected for the real and imaginary parts of anomalous dispersion, taken from ref. 22. In compounds **2** and **5** all non-H atoms were allowed to vibrate anisotropically. Because of the poor quality of the data only Os atoms of the two independent molecules in **3** were treated anisotropically. Geometrical constraints were applied in **3** to the Os–C, C–O and Os • • • O distances during the refinement, while the arene ligands were refined as rigid bodies. In all species hydrogen atoms were added in calculated positions (C–H 1.08 Å) and refined 'riding' on their corresponding C atoms in **2** and **5**, and as a part of the arene rigid groups in **3**. In compounds **2** and **5** single isotropic parameters for the H(ring) and H(Me) groups were refined [0.08(3), 0.15(8) and 0.07, 0.10 Å^2 in **2** and **5**, respectively], while in **3** the H-atom thermal motion was assigned the value 0.09 Å^2 and not refined. Fractional atomic coordinates of **2**, **3** and **5** are reported in Tables 5, 6 and 7.

Additional material available from the Cambridge Crystallographic Data Centre, comprises H-atom coordinates, thermal parameters and remaining bond lengths and angles.

Acknowledgements

Financial support by Ministero dell'Università e della Ricerca Scientifica e Tecnologica (Italy) is acknowledged, and D. B., F. G. and B. F. G. J. acknowledge NATO for a research grant.

References

1 (*a*) D. Braga, F. Grepioni and P. Sabatino, *J. Chem. Soc., Dalton Trans.*, 1990, 3137; (*b*) D. Braga and F. Grepioni, *Acta Crystallogr., Sect. B*, 1989, **45**, 378; (*c*) D. Braga and F. Grepioni, *Organometallics*, 1991, **10**, 1254.

2 (*a*) D. Braga, C. Gradella and F. Grepioni, *J. Chem. Soc., Dalton Trans.*, 1989, 1721; (*b*) D. Braga and F. Grepioni, *Polyhedron*, 1990, **1**, 53; (*c*) S. Aime, D. Braga, R. Gobetto, F. Grepioni and A. Orlandi, *Inorg. Chem.*, 1991, **30**, 951; (*d*) D. Braga, C. E. Anson, A. Bott, B. F. G. Johnson and E. Marseglia, *J. Chem. Soc., Dalton Trans.*, 1990, 3517; (*e*) C. E. Anson, R. E. Benfield, A. W. Bott, D. Braga and E. Marseglia, *J. Chem. Soc., Chem. Commun.*, 1988, 889; (*f*) D. Braga and F. Grepioni, *J. Chem. Soc., Dalton Trans.*, 1990, 3143.

3 C. H. Holm and J. A. Ibers, *J. Chem. Phys.*, 1959, **30**, 885; S. E. Anderson, *J. Organomet. Chem.*, 1974, **71**, 263; D. F. R. Gilson, G. Gomez, I. S. Butler and P. J. Fitzpatrick, *Can. J. Chem.*, 1983, **61**, 737; I. S. Butler, P. J. Fitzpatrick, D. F. R. Gilson, G. Gomez and A. Shaver, *Mol. Cryst. Liq. Cryst.*, 1981, **71**, 213; P. D. Harvey, I. S. Butler and D. F. R. Gilson, *Inorg. Chem.*, 1986, **25**, 1009; A. J. Campbell, C. A. Fyfe, D. Harold-Smith and K. R. Jeffrey, *Mol. Cryst. Liq. Cryst.*, 1976, **36**, 1; C. E. Cohrell, C. A. Fyfe and C. V. Senoff, *J. Organomet. Chem.*, 1972, **43**, 203; A. J. Campbell, C. E. Cotrell, C. A. Fyfe and K. R. Jeffrey, *Inorg. Chem.*, 1976, **15**, 1321; P. Delise, G. Allegra, E. R. Monaschi and A. Chierico, *J. Chem. Soc., Faraday Trans. 2*, 1975, 207.

4 E. Maverick and J. D. Dunitz, *Mol. Phys.*, 1987, **62**, 451; K. Chhor, G. Lucazeau and C. Sourisseau, *J. Raman Spectrosc.*, 1981, **11**, 183; C. H. Holm and J. A. Ibers, *J. Chem. Phys.*, 1959, **30**, 885; A. J. Campbell, C. A. Fyfe, D. Harold-Smith and K. R. Jeffrey, *Mol. Cryst. Liq. Cryst.*, 1976, **36**, 1; A. Kubo, R. Ikeda and D. Nakamura, *Chem. Lett. Jpn.*, 1981, 1497; A. B. Gardner, J. Howard, T. C. Waddington, R. M. Richardson and J. Tomkinson, *Chem. Phys.*, 1981, **57**, 453; C. Sourisseau, A. J. Dianoux and C. Poinsignon, *Mol. Phys.*, 1983, **48**, 367.

5 (*a*) D. Braga and F. Grepioni; *Organometallics*, 1991, **10**, 1260; (*b*) D. Braga, F. Grepioni, B. F. G. Johnson, J. Lewis and M. Martinelli, *J. Chem. Soc., Dalton Trans.*, 1990, 1847.

6 M. A. Gallop, M. P. Gomez-Sal, C. E. Housecroft, B. F. G. Johnson, J. Lewis, S. M. Owen, P. R. Raithby and A. H. Wright, *J. Am. Chem. Soc.*, in the press.

7 H. Chen, B. F. G. Johnson, J. Lewis, D. Braga, F. Grepioni and E. Parisini, *J. Chem. Soc., Dalton Trans.*, 1991, 215.

8 A. I. Kitaigorodsky, *Molecular Crystal and Molecules*, Academic Press, New York, 1973; A. J. Pertsin and A. I. Kitaigorodsky, *The Atom–Atom Potential Method*, Springer, Berlin, 1987.

9 A. Gavezzotti and M. Simonetta, *Organic Solid State Chemistry*, ed. G. R. Desiraju, Elsevier, 1987; *Chem. Rev.*, 1981, **82**, 1.

10 K. Mirsky, *Procedings of the International Summer School on Crystallographic Computing*, Delf University Press, Twente, 1978, p. 169.

11 A. Gavezzotti, *Nouv. J. Chim.*, 1982, **6**, 443.

12 A. Gavezzotti and M. Simonetta, *Acta Crystallogr., Sect. A*, 1976, **32**, 10, 997.

13 A. Gavezzotti, OPEC, Organic Packing Potential Energy Calculations, University of Milano, Italy; see also, *J. Am. Chem. Soc.*, 1983, **195**, 5220.

14 E. Keller, SCHAKAL 88, Graphical Representation of Molecular Models, University of Freiburg, 1988, FRG.

15 R. Mason and W. R. Robinson, *Chem. Commun.*, 1968, 468.

16 B. F. G. Johnson, R. D. Johnston and J. Lewis, *Chem. Commun.*, 1967, 1057; 1968, 2865; A. Sirigu, M. Bianchi and E. Benedetti, *Chem. Commun.*, 1969, 596.

17 L. J. Farrugia, *Acta Crystallogr., Sect. C*, 1988, **44**, 997.

18 A. Gavezzotti and G. R. Desiraju, *Acta Crystallogr., Sect. B*, 1988, **44**, 427.

19 M. P. Gomez-Sal, B. F. G. Johnson, J. Lewis, P. R. Raithby and A. H. Wright, *J. Chem. Soc., Chem. Commun.*, 1985, 1682.

20 D. Braga and F. Grepioni, *Organometallics*, in the press.

21 (*a*) G. M. Sheldrick, SHELX 76, Program for Crystal Structure Determination, University of Cambridge, 1976; (*b*) N. Walker and D. Stuart, *Acta Crystallogr., Sect. B*, 1983, **39**, 158.

22 *International Tables for X-Ray Crystallography*, Kynoch Press, Birmingham, 1975; vol. 4, pp. 99–149.

Received 11*th February* 1991; *Paper* 1/00617G